

Variational Tensor Wavefunctions for the Interacting Quantum Spin Hall Phase

Yixin Ma, Shenghan Jiang,^{*} and Chao Xu[†]

Kavli Institute for Theoretical Sciences, University of Chinese Academy of Sciences, Beijing 100190, China

The quantum spin hall (QSH) phase, also known as the two-dimensional topological insulator, hosts helical edge modes protected by time-reversal symmetry. While first proposed as a band insulator, this phase can also be realized in strongly-correlated systems, where the band theory fails to be a good description. To simulate such a phase in realistic correlated models, it is necessary to provide a generic variational ansatz for the interacting QSH phase. In this work, we propose a framework to construct variational wavefunctions for this phase using fermionic tensor network states. Based on the exactly solvable model built from commuting projectors, we construct a tensor representation of the fixed point wavefunction and extract a set of tensor equations describing symmetry transformation rules on this tensor network. From these equations, we derive the anomalous edge theory, which indicates that such equations indeed give a complete description of the phase. Solutions of tensor equations then give variational ansatz for the QSH phase. Our method would serve as the first step to simulate this phase with tensor algorithms in strongly-correlated systems.

Introduction.— Since the discovery of the quantum spin Hall (QSH) phase¹, it becomes an exciting research direction for studying interplay between symmetry and topology in quantum materials^{2,3}. The QSH phase is first proposed as a topological band insulator, which is characterized by the anomalous helical edge mode and topological response function to external electromagnetic field⁴. As these two properties are both stable against interaction, the QSH phase may also be realized as a Mott insulator in strongly-correlated systems. Indeed, the interacting QSH phase is an example of fermionic symmetry-protected topological (SPT) phases^{5–18}. Recently, various interacting fermionic SPT phases, including the interacting QSH phase, are constructed using commuting-projector Hamiltonians^{19–24}. However, such solvable models only provide fixed-point wavefunctions, and are hardly useful for numerical simulations.

To construct generic variational wavefunctions beyond the fixed point, we turn to fermionic tensor networks^{25–33}. Our strategy is presented as following. Motivated by the interacting edge theory, we introduce the fixed-point wavefunction proposed in Ref. 24, and then translate it to the tensor network state. With such tensor representation, we extract a set of tensor equations for symmetry actions on tensors. From tensor equations, we obtain algebraic data characterizing the anomalous edge theory of the QSH phase. It proves that such tensor equations are sufficient conditions for expressing tensor wavefunctions of the QSH phase. Finally, we apply our method to a spin-1/2 fermionic system on the square lattice: by listing and solving tensor equations, we get variational ansatz for the QSH phase on such system.

Interacting edge theory.— The QSH phase hosts charge conservation symmetry generated by n_f and time reversal symmetry \mathcal{T} , where

$$\mathcal{T}^2 = \exp[i\pi n_f] \equiv F, \quad \mathcal{T} \cdot n_f \cdot \mathcal{T}^{-1} = n_f. \quad (1)$$

Here, F is the fermion parity operator.

To get intuition about the interacting bulk wavefunction, we start from its anomalous edge states. In the

low-energy limit, the edge theory is described by massless helical Dirac fermions:

$$H_{edge} = \int dx (-i v_F) [\psi_R^\dagger(x) \partial_x \psi_R(x) - \psi_L^\dagger(x) \partial_x \psi_L(x)],$$

where $\psi_{L/R}$ is the left/right moving fermion mode, and v_F the fermion velocity. \mathcal{T} acts as $\psi_R \rightarrow i\psi_L$, $\psi_L \rightarrow -i\psi_R$, which forbids mass terms opening a gap.

The interacting edge theory can be analyzed by the bosonization method³⁴. We introduce conjugate fields $\phi(x)$ and $\theta(x)$, both taking value in $[0, 2\pi)$, where $[\partial_x \theta(x), \phi(x')] = 2\pi i \delta(x - x')$. In this language, $\psi_{R/L}(x) \sim \exp[-(i\phi(x) \pm i\theta(x)/2)]$, charge density $\delta\rho(x) = -\partial_x \theta(x)/2\pi$, and current density $j(x) = \partial_t \theta(x)/2\pi$. Symmetry actions on θ and ϕ are derived from its action on $\psi_{R/L}$:

$$\begin{aligned} U(\varphi) : \phi &\rightarrow \phi + \varphi, \quad \theta \rightarrow \theta; \\ \mathcal{T} : \phi &\rightarrow -\phi, \quad \theta \rightarrow \theta + \pi, \quad i \rightarrow -i. \end{aligned} \quad (2)$$

Lagrangian density for the interacting edge theory is^{35,36}

$$\mathcal{L}_{edge} = \frac{1}{2\pi} \partial_x \theta \partial_t \phi - \frac{v_F}{4\pi} \left(\frac{1}{K} (\partial_x \theta)^2 + K (\partial_x \phi)^2 \right) + \dots \quad (3)$$

where K is the Luttinger parameter, and for the non-interacting case $K = 2$. Symmetric scattering terms are presented as \dots in Eq. (3). From Eq. (2), the most relevant scattering term respecting all symmetries is $\alpha \cos(2\theta - 2\theta_0)$, where α , θ_0 depends on microscopic details.

The scaling dimension for $\cos(2\theta - 2\theta_0)$ equals $2K$, and becomes relevant when $K < 1$, driving edge to a gapped phase. The classical configuration for this phase is obtained by minimizing $\alpha \cos(2\theta - 2\theta_0)$. Assuming $\alpha > 0$, ground states are doubly degenerate, characterized by $\langle \theta \rangle = \theta_0$ and $\langle \theta \rangle = \theta_0 + \pi$ respectively. According to Eq. (2), \mathcal{T} exchange these two states, and thus the gapped phase spontaneously break \mathcal{T} symmetry.

Topological defects of such edge symmetry breaking phase host anomalous properties. We consider a time

reversal domain wall at x_0 , with domains $\langle \theta(x < x_0 - \epsilon) \rangle = \theta_0$ and $\langle \theta(x > x_0 + \epsilon) \rangle = \theta_0 + \pi$, as shown in Fig. 1. For region $(x_0 - \epsilon, x_0 + \epsilon)$, θ rotate clockwise/counter-clockwise. Such domain wall carries $\pm 1/2$ charge³⁷, as

$$\int_{x_0-\epsilon}^{x_0+\epsilon} dx \delta\rho(x) = \int_{x_0-\epsilon}^{x_0+\epsilon} dx \left(-\frac{\partial_x \theta(x)}{2\pi} \right) = \pm \frac{1}{2}. \quad (4)$$

The fixed-point wavefunction.- We now extend θ -field to bulk. The clockwise/counter-clockwise domain wall at edge is identified as $\pm 1/2$ vortex, as shown in Fig. 1. The half-charge edge domain wall motivates a decorated vortex picture^{38,39}: each vortex core carries fermions with $n_f = n_w$, where n_w is the winding number. Note that any θ configuration breaks \mathcal{T} , and \mathcal{T} symmetry is recovered by proliferating vortices, where fermion charge is conserved during this process due to conservation of total vorticity.

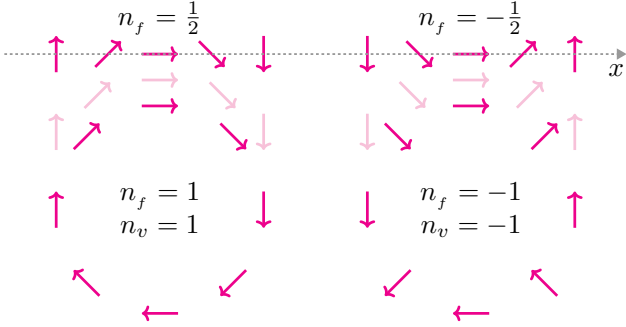


FIG. 1. Edge domain walls and bulk vortex of θ -field with fermion decoration. An edge domain wall of the QSH phase is $\pm\pi$ -rotation of θ -field, carrying $\pm 1/2$ charge. Each bulk vortex is decorated with fermions, where $n_f = n_w$.

Equipped with the decorated vortex picture, we introduce the fixed-point wavefunction²⁴. As in Fig. 2, we consider a system with two types of local degrees of freedom: spin-1/2 fermions f_σ 's at a honeycomb lattice, and Ising spins $|\tau\rangle$'s at the dual triangular lattice, where $\sigma, \tau = \uparrow / \downarrow$. \mathcal{T} flips both spins:

$$\mathcal{T} : |\uparrow\rangle \leftrightarrow |\downarrow\rangle, \quad f_\sigma \rightarrow \sigma_{\sigma\sigma'}^y f_{\sigma'}, \quad i \rightarrow -i. \quad (5)$$

Here, Ising spins mimic θ -field. To distinguish $\pm\pi$ rotation of Ising spins, we add arrows on bonds of the dual lattice: θ rotate $\pm\pi$ when crossing an Ising domain wall along/against the arrow. For arrow convention in Fig. 2, whenever an Ising domain wall goes through a site with sublattice index u/v , $n_w = \pm 1$ at this site. To match n_w , fermions at site $\mathbf{r}s$ are holes/electrons:

$$[n_f, f_{\mathbf{r}s, \sigma}] = -(-1)^s f_{\mathbf{r}s, \sigma}, \quad (6)$$

where \mathbf{r} is the unit cell coordinate, and $(-1)^s = \pm 1$ for $s = u/v$.

The fermion spin at a vortex center is enforced to follow the majority Ising spins at adjacent plaquettes, as shown in Fig. 2. It indicates that at each domain wall loop,

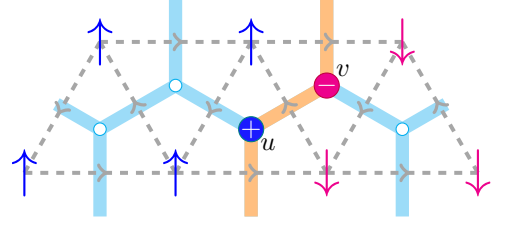


FIG. 2. A typical configuration for the fixed-point wavefunction of the QSH phase. f_σ lives at a honeycomb lattice, while $|\tau\rangle$ at the dual lattice. Spin up/down is colored blue/red. One adds $\pm\pi$ when crossing an Ising domain wall along/against oriented bonds of the dual lattice. For arrows convention presented here, whenever a domain wall across a site with sublattice index u/v , one gets a vortex/anti-vortex decorated with a hole/electron at this site. Spins of fermions follows the majority rule, as indicated by the color.

number of f_\uparrow differs from number of f_\downarrow by ± 6 . Let $|c\rangle$ be a product state of Ising spins and $|\psi_c\rangle$ the corresponding decorated fermion state. With Eq. (5), we then have

$$\mathcal{T}|\psi_c\rangle = (-1)^{N_{dw}(c)}|\psi_{\mathcal{T}c}\rangle, \quad (7)$$

where N_{dw} is the number of domain wall loops in c .

The fixed-point wavefunction is expressed as²⁴

$$|\Psi\rangle = \sum_c \Psi(c)|c\rangle \otimes |\psi_c\rangle, \quad (8)$$

where $\Psi(c) = \pm 1$ satisfies $\Psi(c) = (-1)^{N_{dw}(c)}\Psi(\mathcal{T}c)$ ⁴⁰.

Tensor network representation.- To simulate the interacting QSH phase in realistic models, it is desirable to construct variational wavefunctions beyond Eq. (8). In the following, we develop a framework to get variational ansatz for the QSH phase by fermionic projected entangled-pair states (fPEPS).

fPEPS are built from fermionic tensors, which are quantum states in fermionic tensor product (\otimes_f) of physical and internal legs. Legs with inward/outward arrows are fermionic Hilbert spaces for ket/bra states. By connecting outward and inward internal legs, one contracts states with operation fTr , defined as

$$\text{fTr}[\langle i| \otimes_f |j\rangle] = (-1)^{|i||j|} \text{fTr}[|j\rangle \otimes_f \langle i|] = \delta_{ij} \quad (9)$$

where $(-1)^{|i|}$ ($|i| = 0/1$) is the fermion parity of state $|i\rangle/\langle i|$. Physical wavefunctions for fPEPS are obtained by contracting all internal legs. Typical site and bond tensors for fPEPS on honeycomb lattice are drawn in Fig. 3. All site and bond tensors are set to be *parity even* in this paper. More details about fermionic tensor networks are represented in Sec. I of Supplemental Materials (SM)⁴¹.

Let us work out fPEPS representation of the fixed-point wavefunction in Eq. (8). Imposing translational symmetry, we focus on tensors in one unit cell, including site tensors \hat{T}_u/\hat{T}_v and bond tensors $\hat{B}_x/\hat{B}_y/\hat{B}_z$, as in

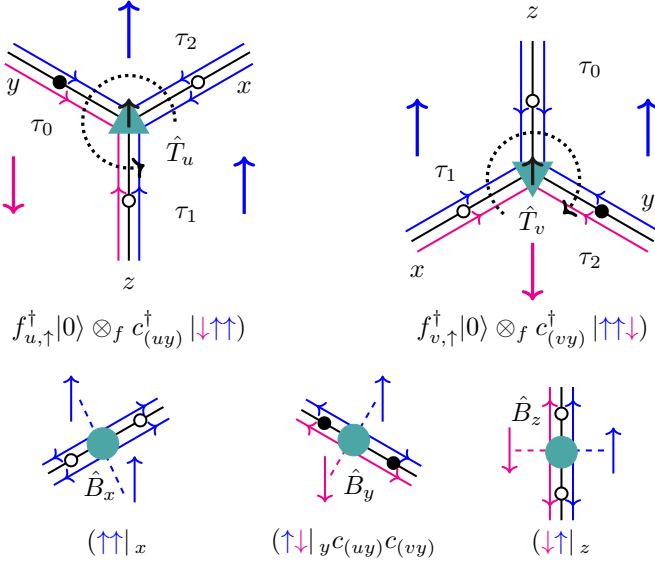


FIG. 3. Representative states for site tensors $\hat{T}_{u/v}$ and bond tensors $\hat{B}_{x/y/z}$. Physical spin-1/2 fermions live at site centers, while two physical Ising spins live at bond centers. Internal legs pointing from bond tensors to site tensors are represented by triple-lines. Lines on two sides of an internal leg are two internal Ising spins $|\tau_0\tau_1\rangle$, where the order follows arrows on dashed arcs. The middle line supports a spinless fermion c , where filled/empty circle represents filled/empty fermion state. Ising spins within a plaquette are set to be the same, and thus are effectively plaquette spins.

Fig. 3. Physical spin-1/2 fermions live at site centers, while two physical Ising spins live at two sides of bond centers. Ising spins within a plaquette are enforced to be the same, and thus are effectively plaquette spins.

Internal leg $(s\alpha)$ is represented as a triple-line, pointing from site s to bond α . The middle line supports a spinless fermion $c_{(s\alpha)}$ with charge $(-1)^{1-s}$, while lines at two sides carry two internal Ising spins. Thus, dimension of leg $(s\alpha)$ equals eight with basis states $(c_{(s\alpha)}^\dagger)^n |\tau_0\tau_1\rangle_{(s\alpha)}$, where fermionic vacuum state $|0\rangle_{(s\alpha)}$ is omitted for brevity. $\tau_0\tau_1$ are ordered counter-clockwise/clockwise around the site u/v , as indicated by arrows on dashed arcs in Fig. 3. Only four basis states $\{|\uparrow\uparrow\rangle_{(s\alpha)}, c_{(s\alpha)}^\dagger |\uparrow\downarrow\rangle_{(s\alpha)}, |\downarrow\uparrow\rangle_{(s\alpha)}, |\downarrow\downarrow\rangle_{(s\alpha)}\}$ will be used in the following construction.

As all spins within a plaquette are the same, a typical state for site tensor \hat{T}_s reads $(f_{s,\uparrow}^\dagger)^{n_\uparrow} (f_{s,\downarrow}^\dagger)^{n_\downarrow} |0\rangle \otimes_f (c_{(sx)}^\dagger)^{n_x} (c_{(sy)}^\dagger)^{n_y} (c_{(sz)}^\dagger)^{n_z} |\tau_1\tau_2\rangle_{(sx)} |\tau_2\tau_0\rangle_{(sy)} |\tau_0\tau_1\rangle_{(sz)}$, which is succinctly expressed as $(f_{s,\uparrow}^\dagger)^{n_\uparrow} (f_{s,\downarrow}^\dagger)^{n_\downarrow} |0\rangle \otimes_f (c_{(sx)}^\dagger)^{n_x} (c_{(sy)}^\dagger)^{n_y} (c_{(sz)}^\dagger)^{n_z} |\tau_0\tau_1\tau_2\rangle$. With this notation,

site tensors for Eq. (8) are

$$\hat{T}_u = |0\rangle \otimes_f [|\uparrow\uparrow\uparrow\rangle + |\downarrow\downarrow\downarrow\rangle] \quad (10)$$

$$+ f_{u,\uparrow}^\dagger |0\rangle \otimes_f [c_{(ux)}^\dagger |\uparrow\uparrow\downarrow\rangle + c_{(uz)}^\dagger |\uparrow\downarrow\uparrow\rangle + c_{(uy)}^\dagger |\downarrow\uparrow\uparrow\rangle] \\ + f_{u,\downarrow}^\dagger |0\rangle \otimes_f [-c_{(uy)}^\dagger |\downarrow\downarrow\uparrow\rangle + c_{(ux)}^\dagger |\downarrow\uparrow\downarrow\rangle - c_{(uz)}^\dagger |\uparrow\downarrow\downarrow\rangle] \\ \hat{T}_v = |0\rangle \otimes_f [|\uparrow\uparrow\uparrow\rangle + |\downarrow\downarrow\downarrow\rangle] \quad (11) \\ + f_{v,\uparrow}^\dagger |0\rangle \otimes_f [c_{(vy)}^\dagger |\uparrow\uparrow\downarrow\rangle + c_{(vx)}^\dagger |\uparrow\downarrow\uparrow\rangle + c_{(vz)}^\dagger |\downarrow\uparrow\uparrow\rangle] \\ + f_{v,\downarrow}^\dagger |0\rangle \otimes_f [c_{(vx)}^\dagger |\downarrow\downarrow\uparrow\rangle - c_{(vz)}^\dagger |\downarrow\uparrow\downarrow\rangle + c_{(vy)}^\dagger |\uparrow\downarrow\downarrow\rangle]$$

Similarly, $\langle\tau_0\tau_1|_\alpha (c_{(u\alpha)})^{n_u} (c_{(v\alpha)})^{n_v}$ is short for a bond state $\langle\tau_0\tau_1|_\alpha \otimes_f (\tau_0\tau_1|_{(u\alpha)} (\tau_1\tau_0|_{(v\alpha)} (c_{(u\alpha)})^{n_u} (c_{(v\alpha)})^{n_v}$. Bond tensors are then expressed as

$$\hat{B}_\alpha = \langle\uparrow\uparrow|_\alpha + \langle\downarrow\downarrow|_\alpha + \langle\downarrow\uparrow|_\alpha - \langle\uparrow\downarrow|_\alpha c_{(u\alpha)} c_{(v\alpha)} \quad (12)$$

As we show in Sec. II of SM⁴¹, two \mathcal{T} -related state from contracting fPEPS satisfy Eq. (7), so this fPEPS indeed gives the fixed-point wavefunction.

Tensor equations.— We extract symmetry transformation rules on internal legs, which pave the way for wavefunctions beyond Eq. (8). We assume that symmetry action on physical legs can be pushed to gauge transformation on internal legs⁴², see also SM⁴¹.

- We note that $c_{(s\alpha)}$ carries charge $(-1)^{1-s}$, while $f_{s,\sigma}$ carries charge $(-1)^s$. All tensors are charge neutral from Eq. (11) and (12):

$$\left(n_{f;s} + \sum_{\alpha=x,y,z} n_{f;(s\alpha)}\right) \cdot \hat{T}_s = \hat{B}_\alpha \cdot \left(\sum_{s=u,v} n_{f;(s\alpha)}\right) = 0$$

So, the physical wavefunction from contracting the fPEPS is also charge neutral.

- \mathcal{T} action on internal ket leg $(s\alpha)$ can be set as

$$W_{(s\alpha)}(\mathcal{T}) = |\uparrow\uparrow\rangle_{(s\alpha)} \langle\downarrow\downarrow|_{(s\alpha)} + |\downarrow\downarrow\rangle_{(s\alpha)} \langle\uparrow\uparrow|_{(s\alpha)} \quad (13) \\ + i c_{(s\alpha)}^\dagger |\uparrow\downarrow\rangle_{(s\alpha)} \langle\downarrow\uparrow|_{(s\alpha)} + |\downarrow\uparrow\rangle_{(s\alpha)} \langle\uparrow\downarrow|_{(s\alpha)} c_{(s\alpha)}$$

which gives the following symmetric condition:

$$\hat{T}_s = U_s(\mathcal{T}) \otimes_f W_{(sx)}(\mathcal{T}) \otimes_f W_{(sy)}(\mathcal{T}) \otimes_f W_{(sz)}(\mathcal{T}) \cdot \hat{T}_s^* \\ \hat{B}_\alpha = V_{(\alpha 0)}(\mathcal{T}) \otimes_f V_{(\alpha 1)}(\mathcal{T}) \cdot \hat{B}_\alpha^* \cdot W_{(v\alpha)}^{-1}(\mathcal{T}) \otimes_f W_{(u\alpha)}^{-1}(\mathcal{T}) \quad (14)$$

Here, $U(\mathcal{T})$ and $V(\mathcal{T})$ are \mathcal{T} -action on physical legs defined in Eq. (5). However, as $W(\mathcal{T})$'s are not parity even, Eq. (14) may not lead to a \mathcal{T} -symmetric wavefunction (see SM⁴¹). In SM⁴¹ Sec. III, we prove that Eq. (14) indeed gives a \mathcal{T} -symmetric condition, which is related to a hidden Kasteleyn orientation^{19,20,43,44}.

- We define $n_{\lambda;(s\alpha a)} = (-1)^{s+a}|\downarrow\rangle\langle\downarrow|$, where $a = 0/1$ labels two side lines of internal leg $(s\alpha)$. We have

$$\begin{aligned} (n_{\lambda;(s\alpha 0)} + n_{\lambda;(s\tilde{\alpha} 1)}) \cdot \hat{T}_s &= 0, \\ \hat{B}_\alpha \cdot (n_{\lambda;(u\alpha a)} + n_{\lambda;(v\alpha a)}) &= 0, \end{aligned} \quad (15)$$

where $\alpha = 0/1/2$ for $x/y/z$ and $\tilde{\alpha} = \alpha - (-1)^s$. Eq. (15) comes from the plaquette spin constraint. n_λ 's action on internal legs within a plaquette p generates a $U(1)$ symmetry. We thus get $[U(1)]^{N_p}$ symmetry, where N_p is the number of plaquettes. Such symmetry acts trivially on physical legs, and is called “invariant gauge group” (IGG)^{45–47}, which is related to topological properties of the phase^{29,48,49} (see also SM⁴¹).

Let us extract group relations between n_f , $W(\mathcal{T})$ and n_λ , which are coined as *tensor equations* in this work. Roughly speaking, IGG gives possible action of the identity element for symmetry group on internal legs. So, symmetry on internal legs satisfy Eq. (1) up to some IGG element^{45–47}. Indeed, from Eq. (13), the commutator between n_f and \mathcal{T} on internal legs reads

$$W_{(s\alpha)}(\mathcal{T}) \cdot n_{f;(s\alpha)} \cdot W_{(s\alpha)}^{-1}(\mathcal{T}) = n_{f;(s\alpha)} + n_{D;(s\alpha)} \quad (16)$$

where $n_{D;(s\alpha)}$ generates a “global” $U(1)$ IGG acting on all internal legs

$$\begin{aligned} n_{D;(s\alpha)} &= (-1)^s (|\downarrow\uparrow\rangle\langle\downarrow\uparrow| - |\uparrow\downarrow\rangle\langle\uparrow\downarrow|) \\ &= n_{\lambda;(s\alpha 0)} + n_{\lambda;(s\alpha 1)} \end{aligned} \quad (17)$$

Physically, n_D gives a $U(1)$ gauge theory. However, the second line of Eq. (17) kills the gauge theory, leading to short-range entangled phase⁴¹.

For group relation $\mathcal{T}^2 = F$, a naïve insertion of an IGG element does not give the correct result for internal legs. Instead, from Eq. (13) and (17), we have

$$\exp\left[i\frac{\pi}{2}n_{D;(s\alpha)}^2\right] \cdot W_{(s\alpha)}(\mathcal{T}) \cdot W_{(s\alpha)}^*(\mathcal{T}) = F_{(s\alpha)} \quad (18)$$

In Sec. IV of SM⁴¹, we show that Eq. (18) is indeed consistent with $\mathcal{T}^2 = F$.

It is also important to calculate the commutator between $W(\mathcal{T})$ and n_λ , which gives

$$W_{(s\alpha)}(\mathcal{T}) \cdot n_{\lambda;(s\alpha a)}^* \cdot W_{(s\alpha)}^{-1}(\mathcal{T}) = -n_{\lambda;(s\alpha a)} + (-1)^{s+a} \quad (19)$$

Edge theories from tensor equations.— In the following, we will show that tensor equations from Eq. (16) to Eq. (19) contain all information for the fPEPS representation of the QSH phase by extracting the anomalous edge theory from these equations.

The anomalous edge theory can be characterized by fusion of two \mathcal{T} -flux⁵⁰. To see this, we turn to the edge

theory in Eq. (3). By rotating $\theta(x)$ by 2π angle counter-clockwise within region $[x_0, x_1]$, we get current density

$$\int dt j(x) = \int dt \frac{\partial_t \theta}{2\pi} = \begin{cases} 0 & x \leq x_0 \text{ or } x \geq x_1 \\ 1 & x_0 < x < x_1 \end{cases} \quad (20)$$

So, a unit charge is pumped from x_0 to x_1 ^{51,52}. According to Eq. (2), rotating θ by π on $[x_0, x_1]$ is equivalent to acting \mathcal{T} on this segment, which creates \mathcal{T} -flux at two ends⁵³. The unit charge pumping due to 2π rotation of θ is interpreted as *two \mathcal{T} -flux fuses to an electron/hole*.

We now extract such fusion rule tensor equations. As in Fig. 4, to obtain edge theory of system A , we cut tensors within A from the infinite fPEPS, and contract all internal legs within A to obtain a large tensor \hat{T}_A . \hat{T}_A has L boundary legs labeled by index $j \in \partial A = \{1, 2, \dots, L\}$, forming Hilbert space $\mathbb{H}_{\partial A}$. As shown in Sec. V of SM⁴¹, the edge Hilbert space \mathbb{H}_{edge} contains states in $\mathbb{H}_{\partial A}$ that are invariant under IGG action. Let P_{edge} be the projector from $\mathbb{H}_{\partial A}$ to \mathbb{H}_{edge} . In our case, P_{edge} identifies Ising spins belonging to the same plaquette: $\tau_{j+\frac{1}{4}} = \tau_{j+\frac{3}{4}}$, where $\tau_{j\pm\frac{1}{4}}$ are Ising spins at boundary leg j .

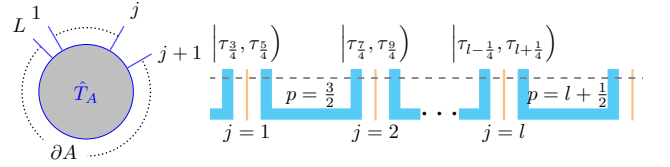


FIG. 4. Left: Tensor \hat{T}_A cutting from the infinite fPEPS, whose boundary legs are numbered from 1 to L . Right: Details of boundary legs of \hat{T}_A . Leg j is a triple-line, representing two Ising spins (thick blue line) $\tau_{j-\frac{1}{4}}$ and $\tau_{j+\frac{1}{4}}$, and one spinless fermion c_j (thin orange line). Plaquette between j and $j+1$ are labeled as $p = j + \frac{1}{2}$.

By projecting $W_{\partial A}(\mathcal{T}) \equiv \bigotimes_{j \in \partial A} W_j(\mathcal{T})$ to \mathbb{H}_{edge} , one gets \mathcal{T} action on edge:

$$U_{edge}(\mathcal{T})\mathcal{K} = W_{\partial A}(\mathcal{T})\mathcal{K} \cdot P_{edge} \quad (21)$$

Let $M = \{2, 3, \dots, l\}$ be a subregion of ∂A , and \mathcal{T} -flux at ends of M are created by a charge-neutral string operator $U_M(\mathcal{T})\mathcal{K}$, where

$$U_M(\mathcal{T})\mathcal{K} = P_{edge} \cdot w_{l+1} \cdot w_1 \cdot W_M(\mathcal{T})\mathcal{K} \cdot P_{edge} \quad (22)$$

Here, $w_{1/(l+1)}$ are local operators on leg $1/(l+1)$, which satisfies the following conditions from the charge-neutral requirement for $U_M(\mathcal{T})\mathcal{K}$ ⁴¹

$$[w_1, n_{f;1}] = n_{\lambda; \frac{3}{2}}^{(0)} \cdot w_1; [w_{l+1}, n_{f;l+1}] = n_{\lambda; l+\frac{1}{2}}^{(1)} \cdot w_{l+1}, \quad (23)$$

where $n_{\lambda;p}^{(0/1)}$ are IGG elements acting on $|\tau_{p\mp\frac{1}{4}}\rangle$.

Without loss of generality, let $j = 1$ and $l+1$ to be v

sublattice, and $w_{1/(l+1)}$ can be solved as

$$w_1 = \sum_{\tau_{\frac{3}{4}}} c_1 \left| \tau_{\frac{3}{4}}, \downarrow_{\frac{5}{4}} \right\rangle \left(\left| \tau_{\frac{3}{4}}, \uparrow_{\frac{5}{4}} \right\rangle + \left| \tau_{\frac{3}{4}}, \uparrow_{\frac{5}{4}} \right\rangle \right) \left(\tau_{\frac{3}{4}}, \downarrow_{\frac{5}{4}} \right| ;$$

$$w_{l+1} = \sum_{\tau_{l+\frac{5}{4}}} c_{l+1}^{\dagger} \left| \downarrow_{l+\frac{3}{4}}, \tau_{l+\frac{5}{4}} \right\rangle \left(\left| \uparrow_{l+\frac{3}{4}}, \tau_{l+\frac{5}{4}} \right| \right.$$

$$\left. + \left| \uparrow_{l+\frac{3}{4}}, \tau_{l+\frac{5}{4}} \right\rangle \right) \left(\downarrow_{l+\frac{3}{4}}, \tau_{l+\frac{5}{4}} \right| . \quad (24)$$

It is then straightforward to get

$$[U_M(\mathcal{T})\mathcal{K}]^2 = P_{edge} \cdot \Omega_1 \cdot \Omega_{l+1} \cdot \prod_{j=2}^l F_j \cdot P_{edge} \quad (25)$$

Here, $\Omega_{1/(l+1)}$ are interpreted as quasi-particles obtained by fusing two T -flux: $\Omega_1 = c_1 \exp \left[i \frac{\pi}{2} \cdot n_{\lambda; \frac{3}{2}}^{(1)} \right]$ creates a hole and $\Omega_{l+1} = c_{l+1}^{\dagger} \exp \left[-i \frac{\pi}{2} \cdot n_{\lambda; l+\frac{1}{2}}^{(0)} \right]$ creates an electron (see details in SM Sec. VI⁴¹). We recover the anomalous edge theory, which suggests that any fPEPS that satisfies tensor equations belongs to the QSH phase⁵⁴.

Variational tensor wavefunctions.- The above honeycomb example is quite artificial, as it requires both spin-1/2 fermions as well as additional plaquette Ising spins. In the following, let us consider a spin-1/2 fermion system on a square lattice, where electrons and holes live on different sublattices of this bipartite lattice. We try to obtain variational ansatz for the QSH phase by solving tensor equations.

There are two types of site tensors and four types of bond tensors on this bipartite square system. Each site tensor has one physical and four internal legs: $\hat{T}_s = (T_s)_{ijkl,p} |i\rangle_{(s1)} |j\rangle_{(s2)} |k\rangle_{(s3)} |l\rangle_{(s4)} |p\rangle_s$, with $s = u/v$ labeling the sublattices, and subindices 1 to 4 ordering internal legs clockwise. A physical leg supports a spin-1/2 fermion f_σ , and charges carried by f_σ 's are opposite in sublattices u and v . For simplicity, we choose basis of an internal leg ($s\alpha$) to be the same as the honeycomb example: $\left\{ |\uparrow\uparrow\rangle_{(s\alpha)}, c_{(s\alpha)}^{\dagger} |\uparrow\downarrow\rangle_{(s\alpha)}, |\downarrow\uparrow\rangle_{(s\alpha)}, |\downarrow\downarrow\rangle_{(s\alpha)} \right\}$.

Action of \mathcal{T} on physical legs follows Eq. (5). Symme-

tries pose constraints on site tensor \hat{T}_s as

$$\bigotimes_{\alpha=1}^4 W_{(s\alpha)}(\mathcal{T}) \otimes_f U_s(\mathcal{T}) \cdot \hat{T}_s^* = \hat{T}_s$$

$$\left[\sum_{\alpha=1}^4 n_{f;(s\alpha)} + n_{f;s} \right] \cdot \hat{T}_s = 0. \quad (26)$$

In addition, site tensors should also be invariant under plaquette IGG n_λ 's, as in Eq. (15). $W(\mathcal{T})$, n_f and n_λ satisfy tensor equations from Eq. (16) to (19), and can simply take the same form as in the honeycomb example. By solving these tensor constraints, we obtain 14 linearly independent solutions for $\hat{T}_{u/v}$, as listed in SM Sec. VII⁴¹. Bond tensors are set to be Eq. (12), which satisfy all tensor equations⁴¹.

Discussion.- In this work, by representing the fixed-point wavefunction of the QSH phase with fPEPS, we extract tensor equations from Eq. (16) to (19). By solving tensor equations, we can obtain general forms for symmetry actions on internal legs. Variational ansatz for the QSH phase are solved by imposing such symmetry constraints on local tensors.

The work leaves several interesting future directions. To express variational ansatz for topological phases on half-filled spin-1/2 *electronic* models, it is necessary to generalize our framework to tensors with odd parity. To simulate the QSH phase in strongly correlated models, it is desirable to develop variational numerical algorithms for symmetric fPEPS wavefunctions obtained here. On the analytical side, we would like to consider other fermionic topological phases, including topological superconductors and topologically ordered phases. The most interesting case would be the chiral phases such as $p+ip$ topological superconductor^{55–57}: it remains a puzzle whether fPEPS are capable to represent these chiral phases with finite bulk gap^{58–60}. Besides, spatial symmetries can be easily encoded in tensor networks⁴⁶, which enable us to construct variational tensor wavefunctions for gapped electronic liquid phases and high-order topological insulators/superconductors⁶¹.

We would like to thank Qing-Rui Wang and Xie Chen for helpful discussions. The work is supported by MOST NO. 2022YFA1403901, NSFC NO. 12104451, and funds from Strategic Priority Research Program of CAS (No. XDB28000000).

* jiangsh@ucas.ac.cn

† xuchao@ucas.ac.cn

¹ C. L. Kane and E. J. Mele, *Phys. Rev. Lett.* **95**, 226801 (2005).

² X.-L. Qi and S.-C. Zhang, *Rev. Mod. Phys.* **83**, 1057 (2011).

³ M. Z. Hasan and C. L. Kane, *Rev. Mod. Phys.* **82**, 3045 (2010).

⁴ X.-L. Qi, T. L. Hughes, and S.-C. Zhang, *Phys. Rev. B*

78, 195424 (2008).

⁵ L. Fidkowski and A. Kitaev, *Phys. Rev. B* **81**, 134509 (2010).

⁶ L. Fidkowski and A. Kitaev, *Phys. Rev. B* **83**, 075103 (2011).

⁷ X. Chen, Z.-C. Gu, and X.-G. Wen, *Phys. Rev. B* **84**, 235128 (2011).

⁸ Z.-C. Gu and X.-G. Wen, *Phys. Rev. B* **90**, 115141 (2014).

⁹ Z.-C. Gu and M. Levin, *Phys. Rev. B* **89**, 201113 (2014).

- ¹⁰ Q.-R. Wang and Z.-C. Gu, *Phys. Rev. X* **8**, 011055 (2018).
- ¹¹ Q.-R. Wang and Z.-C. Gu, *Phys. Rev. X* **10**, 031055 (2020).
- ¹² C. Wang, C.-H. Lin, and Z.-C. Gu, *Phys. Rev. B* **95**, 195147 (2017).
- ¹³ M. Cheng, N. Tantivasadakarn, and C. Wang, *Phys. Rev. X* **8**, 011054 (2018).
- ¹⁴ C. Wang, A. C. Potter, and T. Senthil, *Science* **343**, 629 (2014).
- ¹⁵ C. Wang and T. Senthil, *Phys. Rev. B* **89**, 195124 (2014).
- ¹⁶ T. Senthil, *Annu. Rev. Condens. Matter Phys.* **6**, 299 (2015).
- ¹⁷ E. Witten, *Rev. Mod. Phys.* **88**, 035001 (2016).
- ¹⁸ D. S. Freed and M. J. Hopkins, *Geometry & Topology* **25**, 1165 (2021).
- ¹⁹ B. Ware, J. H. Son, M. Cheng, R. V. Mishmash, J. Alicea, and B. Bauer, *Phys. Rev. B* **94**, 115127 (2016).
- ²⁰ N. Tarantino and L. Fidkowski, *Phys. Rev. B* **94**, 115115 (2016).
- ²¹ Z. Wang, S.-Q. Ning, and X. Chen, *Phys. Rev. B* **98**, 094502 (2018).
- ²² M. A. Metlitski, “A 1d lattice model for the boundary of the quantum spin-hall insulator,” (2019), [arXiv:1908.08958 \[cond-mat.str-el\]](#).
- ²³ J. H. Son and J. Alicea, *Phys. Rev. B* **100**, 155107 (2019).
- ²⁴ Q.-R. Wang, Y. Qi, C. Fang, M. Cheng, and Z.-C. Gu, “Exactly solvable lattice models for interacting electronic insulators in two dimensions,” (2021), [arXiv:2112.15533 \[cond-mat.str-el\]](#).
- ²⁵ T. Barthel, C. Pineda, and J. Eisert, *Phys. Rev. A* **80**, 042333 (2009).
- ²⁶ P. Corboz, G. Evenbly, F. Verstraete, and G. Vidal, *Phys. Rev. A* **81**, 010303 (2010).
- ²⁷ C. V. Kraus, N. Schuch, F. Verstraete, and J. I. Cirac, *Phys. Rev. A* **81**, 052338 (2010).
- ²⁸ Z.-C. Gu, F. Verstraete, and X.-G. Wen, “Grassmann tensor network states and its renormalization for strongly correlated fermionic and bosonic states,” (2010), [arXiv:1004.2563 \[cond-mat.str-el\]](#).
- ²⁹ N. Schuch, D. Pérez-García, and I. Cirac, *Phys. Rev. B* **84**, 165139 (2011).
- ³⁰ N. Bultinck, D. J. Williamson, J. Haegeman, and F. Verstraete, *Journal of Physics A: Mathematical and Theoretical* **51**, 025202 (2017).
- ³¹ N. Bultinck, D. J. Williamson, J. Haegeman, and F. Verstraete, *Phys. Rev. B* **95**, 075108 (2017).
- ³² C. Wille, O. Buerschaper, and J. Eisert, *Phys. Rev. B* **95**, 245127 (2017).
- ³³ J. I. Cirac, D. Perez-Garcia, N. Schuch, and F. Verstraete, *Reviews of Modern Physics* **93**, 045003 (2021).
- ³⁴ F. Haldane, *Journal of Physics C: Solid State Physics* **14**, 2585 (1981).
- ³⁵ C. Wu, B. A. Bernevig, and S.-C. Zhang, *Phys. Rev. Lett.* **96**, 106401 (2006).
- ³⁶ C. Xu and J. E. Moore, *Phys. Rev. B* **73**, 045322 (2006).
- ³⁷ J. Goldstone and F. Wilczek, *Phys. Rev. Lett.* **47**, 986 (1981).
- ³⁸ X. Chen, Y.-M. Lu, and A. Vishwanath, *Nature communications* **5**, 3507 (2014).
- ³⁹ Z.-X. Liu, Z.-C. Gu, and X.-G. Wen, *Phys. Rev. Lett.* **113**, 267206 (2014).
- ⁴⁰ We mention that to fully determine $|\Psi\rangle$, we should explicitly write down the fermion order and set the ± 1 phase for each $\Psi(c)$ However, such information is quite complicated²⁴ and is unnecessary for the following tensor construction.
- ⁴¹ See Supplemental Material.
- ⁴² D. Pérez-García, M. Sanz, C. Gonzalez-Guillen, M. M. Wolf, and J. I. Cirac, *New Journal of Physics* **12**, 025010 (2010).
- ⁴³ D. Cimasoni and N. Reshetikhin, *Communications in Mathematical Physics* **275**, 187 (2007).
- ⁴⁴ T. D. Ellison and L. Fidkowski, *Phys. Rev. X* **9**, 011016 (2019).
- ⁴⁵ X.-G. Wen, *Phys. Rev. B* **65**, 165113 (2002, [cond-mat/0107071](#)).
- ⁴⁶ S. Jiang and Y. Ran, *Phys. Rev. B* **92**, 104414 (2015).
- ⁴⁷ S. Jiang and Y. Ran, *Phys. Rev. B* **95**, 125107 (2017).
- ⁴⁸ Z.-C. Gu, M. Levin, and X.-G. Wen, *Phys. Rev. B* **78**, 205116 (2008).
- ⁴⁹ N. Schuch, I. Cirac, and D. Pérez-García, *Annals of Physics* **325**, 2153 (2010).
- ⁵⁰ D. V. Else and C. Nayak, *Phys. Rev. B* **90**, 235137 (2014).
- ⁵¹ X.-L. Qi, T. L. Hughes, and S.-C. Zhang, *Nature Physics* **4**, 273 (2008).
- ⁵² L. Fu and C. L. Kane, *Phys. Rev. B* **74**, 195312 (2006).
- ⁵³ X. Chen and A. Vishwanath, *Phys. Rev. X* **5**, 041034 (2015).
- ⁵⁴ It is possible that additional IGG elements emerge in the thermodynamic limit⁶². In such case, fPEPS wavefunction may give other phases, such as spontaneously symmetry breaking phases.
- ⁵⁵ N. Read and D. Green, *Phys. Rev. B* **61**, 10267 (2000).
- ⁵⁶ D. A. Ivanov, *Phys. Rev. Lett.* **86**, 268 (2001).
- ⁵⁷ M. Stone and R. Roy, *Phys. Rev. B* **69**, 184511 (2004).
- ⁵⁸ T. B. Wahl, H.-H. Tu, N. Schuch, and J. I. Cirac, *Phys. Rev. letters* **111**, 236805 (2013).
- ⁵⁹ T. B. Wahl, S. T. Haßler, H.-H. Tu, J. I. Cirac, and N. Schuch, *Phys. Rev. B* **90**, 115133 (2014).
- ⁶⁰ J. Dubail and N. Read, *Phys. Rev. B* **92**, 205307 (2015).
- ⁶¹ A. Rasmussen and Y.-M. Lu, *Phys. Rev. B* **101**, 085137 (2020).
- ⁶² H. Dreyer, L. Vanderstraeten, J.-Y. Chen, R. Verresen, and N. Schuch, “Robustness of critical $u(1)$ spin liquids and emergent symmetries in tensor networks,” (2020), [arXiv:2008.04833 \[cond-mat.str-el\]](#).

Supplementary Materials: Variational Tensor Wavefunctions for the Interacting Quantum Spin Hall Phase

Yixin Ma, Shenghan Jiang,^{*} and Chao Xu[†]

Kavli Institute for Theoretical Sciences, University of Chinese Academy of Sciences, Beijing 100190, China

In this supplemental material, we provide a brief review of fermionic tensor network states (Sec. I), detailed information for the fixed-point tensor network wavefunction of QSH phase (Sec. II), Kasteleyn orientation (Sec. III), detailed derivation of $\mathcal{T}^2 = F$ on internal legs (Sec. IV), edge theory from infinite PEPS (Sec. V), derivation of fusion of \mathcal{T} -flux (Sec. VI), and the variational ansatz for the QSH phase on a square system (Sec. VII).

I. SYMMETRIC FERMIONIC TENSOR NETWORK STATES

In this appendix, we review the fundamentals of fermionic tensor network states^{27,30,31}, and fix our notations used in the main text.

A. Fermionic tensors and tensor contraction

Building blocks of fermionic tensor networks are fermionic tensors, which live in fermionic tensor product (labeled as \otimes_f) of legs. Legs with inward/outward arrows are local fermion Hilbert spaces for ket/bra states, where the parity of state $|i\rangle/\langle i|$ is $(-1)^{|i|}$ with $|i| \in \{0, 1\}$. Exchanging states of two legs gives -1 if these two states are both parity odd:

$$|i\rangle_a \otimes_f |j\rangle_b = (-1)^{|i||j|} |j\rangle_b \otimes_f |i\rangle_a \quad (\text{S1})$$

As an example of fermionic tensors, let us consider tensor \hat{T} with three legs, say a, b, c :

$$\hat{T} = (T_{abc})_{ijk} |i\rangle_a \otimes_f |j\rangle_b \otimes_f |k\rangle_c \quad (\text{S2})$$

Leg indices abc are sometimes ignored when there is no confusion. We may also omit \otimes_f 's and use a more compact form $\hat{T} = T_{ijk} |ijk\rangle$.

Ket and bra states can be contracted using fTr , defined as

$$\text{fTr}[|i\rangle \otimes_f |j\rangle] = (-1)^{|i||j|} \text{fTr}[|j\rangle \otimes_f |i\rangle] = \delta_{ij} \quad (\text{S3})$$

It is noteworthy that the order of contracted states matters as extra -1 may be produced. Generalization to tensor contractions is straightforward. As shown in Fig. 1, for two fermionic tensors $\hat{M} = M^{ijk} |i\rangle_a \langle j|_b \langle k|_c$, $\hat{N} = N_{lm} |l\rangle_d |m\rangle_e$,

$$\text{fTr}_b[\hat{M} \otimes_f \hat{N}] \equiv (-1)^{|j||k|} M^{ijk} N_{lm} \delta_{jl} \langle i| \langle k| | m\rangle \quad (\text{S4})$$

We may omit cumbersome fTr 's and \otimes_f 's and use $\hat{M} \cdot \hat{N}$ to represent tensor contraction.

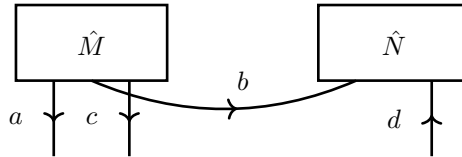


FIG. 1. Graphic representation of contraction between fermionic tensors \hat{M} and \hat{N} . The outward legs are bra spaces and inward legs are ket spaces. The intersection of leg b and c indicates a possible extra minus sign due to exchanging fermions.

For local tensors in tensor network states, there are two types of legs: internal ones and physical ones. States in physical legs is denoted by $|\bullet\rangle/\langle\bullet|$, while states in internal legs by $|\bullet\rangle/(\bullet|$. To get a physical wavefunction, all internal legs are contracted. By fixing parity of all local tensors, physical wavefunctions have fixed parity. In this work, we focus on the case where all local tensors are *parity even*.

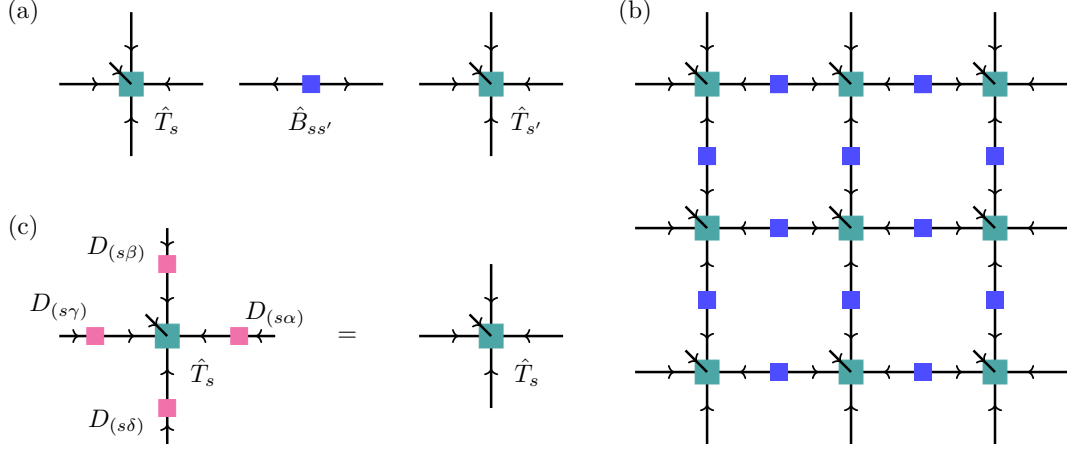


FIG. 2. (a) A bond tensor $\hat{B}_{ss'}$ and its neighbouring site tensors. (b) A 3×3 fPEPS on square lattice with boundary legs. (c) IGG invariance of a single site tensor.

B. Gauge transformation and symmetries of fPEPS

We consider a particular type of fermionic tensor network – fermionic projected entangled-pair state(s) (fPEPS)²⁹. As shown in Fig. 2(a), we focus on fPEPS with both site tensors \hat{T}_s and bond tensors $\hat{B}_{ss'}$, where s, s' label neighbouring site coordinates. Without loss of generality, we assume that internal legs of site tensors all point inward (ket spaces), while those of bond tensors point outward (bra spaces). Physical wavefunction then reads $|\Psi\rangle = \text{fTr} [\mathbb{B} \otimes_f \mathbb{T}]$, where $\mathbb{T} = \bigotimes_{s,f} \hat{T}_s$ and $\mathbb{B} = \bigotimes_{(ss'),f} \hat{B}_{ss'}$. Note that as all tensors are parity even, different orders of tensor contraction give the same state.

Representation of physical wavefunction $|\Psi\rangle$ by fPEPS is far from unique. In particular, two fPEPS represent the same wavefunction if they are related by some gauge transformation:

$$|\psi\rangle = \text{fTr} [\mathbb{B} \otimes_f \mathbb{T}] = \text{fTr} [\mathbb{B} \otimes_f \mathbb{W}^{-1} \otimes_f \mathbb{W} \otimes_f \mathbb{T}] \quad (\text{S5})$$

Here, \mathbb{W} and \mathbb{W}^{-1} are tensor products of gauge transformation W 's on internal legs:

$$\begin{aligned} \mathbb{W} &= W_{(s_1\alpha_1)} \otimes_f W_{(s_1\alpha_2)} \otimes_f \cdots \otimes_f W_{(s_1\alpha_m)} \otimes_f W_{(s_2\alpha_1)} \otimes_f \cdots \otimes_f W_{(s_n\alpha_m)}, \\ \mathbb{W}^{-1} &= W_{(s_n\alpha_m)}^{-1} \otimes_f \cdots \otimes_f W_{(s_n\alpha_1)}^{-1} \otimes_f \cdots \otimes_f W_{(s_{n-1}\alpha_m)}^{-1} \otimes_f \cdots \otimes_f W_{(s_1\alpha_1)}^{-1} \end{aligned} \quad (\text{S6})$$

where $(s\alpha)$ labels internal leg, and

$$W_{(s\alpha)} |i\rangle_{(s\alpha)} = \sum_b [W_{(s\alpha)}]_{ji} |j\rangle_{(s\alpha)}, \quad \langle i|_{(s\alpha)} W_{(s\alpha)}^{-1} = \sum_j \langle j|_{(s\alpha)} [W_{(s\alpha)}^{-1}]_{ij} \quad (\text{S7})$$

W 's in general do not have fixed parity, and thus permuting W 's and W^{-1} 's may lead to fermion swapping gate.

For the case where $|\Psi\rangle$ is invariant under symmetry g , we assume that g -action on physical legs can be pushed to gauge transformation on internal legs of local tensors:

$$U_s(g) \otimes \left(\bigotimes_{\alpha} W_{(s\alpha)}(g) \right) \cdot \hat{T}_s = \hat{T}_s, \quad \hat{B}_{ss'} \cdot W_{(s\alpha)}^{-1}(g) \otimes_f W_{(s'\alpha')}(g) = \hat{B}_{ss'} \quad (\text{S8})$$

where $A \cdot B$ means $\text{fTr}[A \otimes_f B]$. The above equations give symmetry constraints for local tensors. We remark that to get a symmetric wavefunction, orders of $W(g)$'s in the above equation are essential. In particular, as we will show in Appendix III, a valid order of $W(g)$'s gives a Kasteleyn orientation on the lattice.

As shown in Fig. 2(c), there exists a special kind of gauge transformation \mathbb{D} , which leaves every single tensor invariant:

$$\left(\bigotimes_{\alpha} D_{(s\alpha)} \right) \cdot \hat{T}_s = \hat{T}_s, \quad \hat{B}_{ss'} \cdot D_{(s\alpha)}^{-1} \otimes_f D_{(s'\alpha')}^{-1} = \hat{B}_{ss'}. \quad (\text{S9})$$

Such gauge transformation form invariant gauge group (IGG). In this work, we focus on the case where D 's are parity even.

Note that the group always have a trivial center H formed by phase factors $\chi_{(s\alpha)}$ that satisfy $\prod_{(s\alpha)} \chi_{(s\alpha)} = 1$. In addition, if the IGG is a $U(1)$ group generated by $n_{D;(s\alpha)}$, namely, $D_{(s\alpha)}(\theta) = \exp[i\theta n_{D;(s\alpha)}]$. We then have $(\sum_{\alpha} n_{D;(s\alpha)}) \cdot \hat{T}^s = 0$

C. Plaquette IGG and vanishing long-range entanglement

In this work, all internal legs can be further decomposed to tensor product of local Hilbert space:

$$\mathcal{H}_{(s\alpha)} = \bigotimes_a \mathcal{H}_{(s\alpha a)} \quad (\text{S10})$$

Graphically, an internal leg are represented by multiple lines, and we use index a to label lines.

As shown in Fig. 3, we assume that all elements of IGG are parity even and have a “plaquette decomposition”⁴⁷

$$D_{(s\alpha)} = \bigotimes_a D_{(s\alpha a)} \quad (\text{S11})$$

Here, $a = 0/1$ denote lines at two sides.

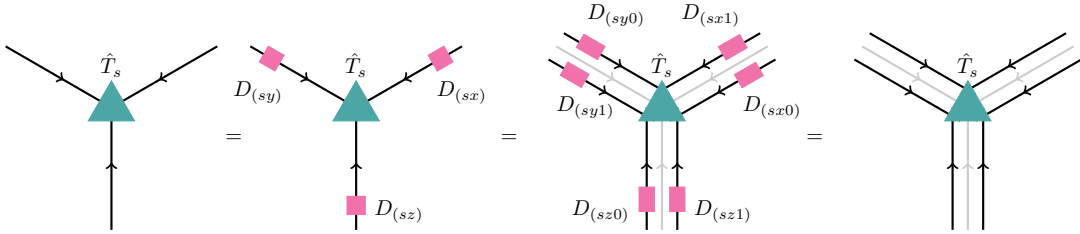


FIG. 3. Any IGG element can be decomposed to plaquette IGG.

In particular, for site tensors on honeycomb lattice, the plaquette IGG action gives

(S12)

Nontrivial IGG element often leads to topological ground state degeneracy. To see this, let us consider a fPEPS with periodic boundary condition on square lattice:

$$|\Psi\rangle = \text{[Diagram of a square lattice tensor network]},$$

The diagram shows a 3x3 grid of blue squares (tensors) connected by solid lines (bonds). Dashed lines form a larger square around the grid, indicating periodic boundary conditions.

where the bond tensors, physical legs and leg orientations are omitted for brevity. If such tensor network has a

nontrivial IGG element, we can insert “IGG loops” in internal legs, which leaves the wavefunction invariant:

$$|\Psi\rangle = \text{[Diagram]} = \text{[Diagram with loops]} = |\Psi\rangle.$$

However, by inserting non-contractible loops of IGG action, we in general obtain a different state as

$$|\Psi_v\rangle = \text{[Diagram]} = \text{[Diagram with loop]} = |\Psi_v\rangle. \quad (\text{S13})$$

$|\Psi_v\rangle$ can't be distinguished with $|\Psi\rangle$ using local operators, as the noncontractible loop can move freely. Thus, if $|\psi\rangle$ is a ground state of a local Hamiltonian, a nontrivial IGG indicates that the Hamiltonian has topological ground state degeneracy. In other words, $|\psi\rangle$ is a long-range entangled state.

However, the plaquette decomposition of the IGG element kills the long-range entanglement. To see this, we apply Eq. (S12) for $|\Psi_v\rangle$ in Eq. (S13), and obtain

$$|\Psi_v\rangle = \text{[Diagram]} = \text{[Diagram with segments]} = \text{[Diagram with thick lines]} = \text{[Diagram with single lines]} = |\Psi\rangle$$

In other words, the non-contractible loop the IGG element acts trivially on the tensor network state if the IGG element has plaquette decomposition. Thus, we obtain a short-range entangled state.

II. TENSOR REPRESENTATION OF THE FIXED-POINT WAVEFUNCTION FOR THE QSH PHASE

In this section, we will prove that the wavefunction constructed from tensors in Eq. (11) and (12) in the main text satisfies \mathcal{T} symmetry.

The wavefunction obtained by contracting all internal legs reads: $|\Psi\rangle = \text{fTr}[\mathbb{T} \otimes_f \mathbb{B}]$. Here,

$$\mathbb{T} = \bigotimes_{\mathbf{r}s} \hat{T}_{(\mathbf{r}s)}, \quad \mathbb{B} = \bigotimes_{\mathbf{r}\alpha} \hat{B}_{\mathbf{r}\alpha}, \quad (\text{S14})$$

where \mathbf{r} is coordinate for unit cell, $s = u/v$, and $\alpha = x/y/z$. The order of tensors is not important since site and bond tensors are all parity even.

Such wavefunction can be organized according to plaquette Ising spin configurations c :

$$|\Psi\rangle = \sum_c \Psi(c) |c\rangle \otimes |\psi_c\rangle \quad (\text{S15})$$

Here, $|c\rangle$ is the quantum state for Ising spin configuration c , and $|\psi_c\rangle$ is the spin-1/2 fermion decoration for c . We choose some fixed order for physical fermion modes, and thus there is no ambiguous sign for $|\psi_c\rangle$. Entries of site and bond tensors in the main take ± 1 , so $\Psi(c)$ also takes ± 1 . In the following, we will show that for any configuration c

and its \mathcal{T} counterpart $\mathcal{T}c$, $\Psi(c) = (-1)^{N_{dw}(c)}\Psi(\mathcal{T}c)$, where $N_{dw}(c)$ is the number of domain wall loops for c . As we argue in Eq. (7) and Eq. (8), such state is symmetric under \mathcal{T} .

For the trivial configuration c where all Ising spins points up, $|\psi_c\rangle$ is vacuum state, and $\Psi(c) = \Psi(\mathcal{T}c) = 1$. Let us consider *configuration c with a single domain wall loop*, and assume this loop contains $2L$ sites and $2L$ bonds. Overlapping $|\Psi\rangle$ with $|c\rangle$, we obtain $\Psi(c)|\psi(c)\rangle$, which is a new tensor network with site tensors $\hat{T}_{\mathbf{r}_s}^c$ and bond tensors $\hat{B}_{\mathbf{r}_\alpha}^c$. Dimension of an internal leg for this new tensor network equals 1, but such internal state can be either boson or fermion state. Site and bond tensors away from the loop contains no fermion, and is a pure spin state with coefficient 1. We focus on tensors in the loop. We label site tensors along the loop as \hat{T}_j^c , where $j = \{1 \cdots 2L\}$, starting from an arbitrary site, and increases clockwise along this loop. Without loss of generality, we choose the $j = 2k - 1$ to be u -sites, and then $j = 2k$ to be v -sites. We use $\hat{B}_{j,j+1}^c$ to label the bond tensor connecting j and $j + 1$. The tensor network to obtain $|\psi(c)\rangle$ is schematically drawn as following:

$$\Psi(c)|\psi(c)\rangle = \text{Diagram}, \quad (\text{S16})$$

where we only present tensors in the domain wall loop. Here, blue legs are physical fermions, and light gray legs are internal spins connecting to tensors within domains. Yellow dots here denote fermion swapping gates. Internal legs traveling from right to left are colored red, and give an additional -1 when contracting odd parity states according to Eq. (S3). $\Psi(\mathcal{T}c)|\psi(\mathcal{T}c)\rangle$ can be drawn in a similar way.

Note that fermion ordering are fixed, and we can then directly compare their coefficients. Coefficients for these two configurations come from two contributions: one from contracting internal fermions, and the other one from the ± 1 entries of tensors. Let us calculate these two contributions respectively in the following.

- We assume that the loop encircles an \uparrow domain. From Eq. (12), $\hat{B}_{2k-1,2k}^c$ contains fermion modes c_{2k-1} and c_{2k} , while $\hat{B}_{2k,2k+1}^c$ carries zero fermion charge. One can read from Eq. (S16) that contraction between $\hat{B}_{2k-1,2k}^c$ and \hat{T}_{2k-1}^c and between $\hat{B}_{2k-1,2k}^c$ and \hat{T}_{2k}^c both give a -1 , and thus total no sign factor.

Configuration $\mathcal{T}c$ hosts a \downarrow domain inside the loop. $\hat{B}_{2k,2k+1}^{\mathcal{T}c}$ contains fermion modes c_{2k} and c_{2k+1} , while $\hat{B}_{2k-1,2k}^{\mathcal{T}c}$ is a pure spin state. From Eq. (S16), one concludes that for $k < L$, the contraction between $\hat{B}_{2k,2k+1}^{\mathcal{T}c}$, $\hat{T}_{2k}^{\mathcal{T}c}$ and $\hat{T}_{2k+1}^{\mathcal{T}c}$ contributes -1 , and the contraction between $\hat{B}_{2L,1}^{\mathcal{T}c}$, $\hat{T}_1^{\mathcal{T}c}$ and $\hat{T}_{2L}^{\mathcal{T}c}$ contributes no phase factor. So, the sign difference between c and $\mathcal{T}c$ from fermion contraction is $(-1)^{L-1}$.

- We now calculate contribution from tensor entries. Given site and bond tensors in the main text, one can check that for any loop with length $2L$, under \mathcal{T} action, there are always L site tensors and $2L$ bond tensors on the loop change signs. This can be seen by noticing that on a domain wall loop there are always same number of u -sites and v -sites that locate between domain walls of an x -bond and a y -bond (or x -bond and z -bond, or y -bond and z -bond), while sign factors of these u - and v -sites are opposite under \mathcal{T} action. Thus, tensor entries contribute $(-1)^L$ to the sign difference between c and $\mathcal{T}c$.

Combining above contributions, we conclude that $\Psi(c) = -\Psi(\mathcal{T}c)$ for c with a single domain wall.

For configurations with multiple domain wall loops, one can first moving tensors belonging to a single loop together. Coefficients for each loop can then be calculated one by one. So, for any configuration c with $N_{dw}(c)$ domain wall loops, we have $\Psi(\mathcal{T}c) = (-1)^{N_{dw}(c)}\Psi(c)$.

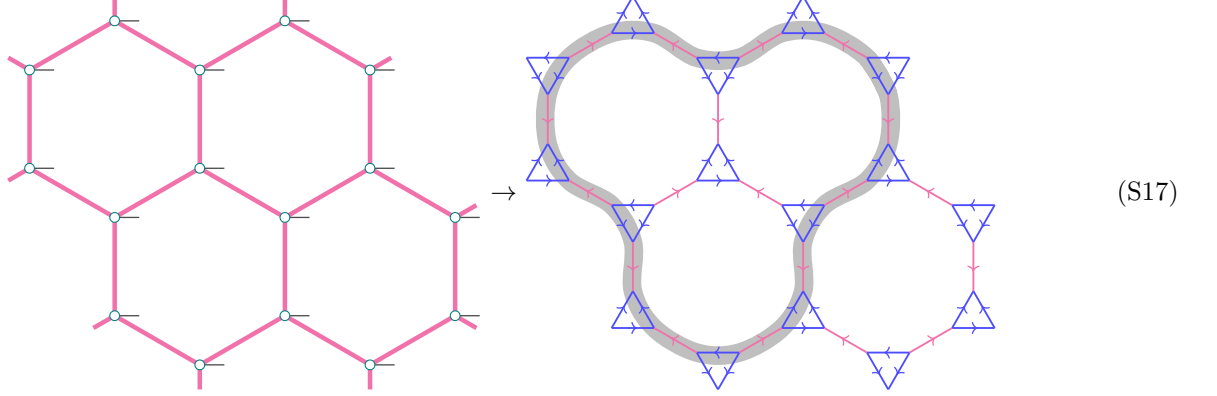
III. TIME REVERSAL SYMMETRY AND KASTELEYN ORIENTATION

When acting \mathcal{T} on the honeycomb fPEPS, we get $W(\mathcal{T})$'s and $W^{-1}(\mathcal{T})$'s on internal legs according to Eq. (14). For any internal leg $(s\alpha)$, $W_{(s\alpha)}(\mathcal{T})$ in general are not in the neighbourhood of $W_{(s\alpha)}^{-1}(\mathcal{T})$, and one need to move them together to cancel each other in the tensor contraction. Since $W(\mathcal{T})$ does not have fixed parity, permuting $W(\mathcal{T})$'s and $W^{-1}(\mathcal{T})$'s lead to fermion-swap gates. So, Eq. (14) in general does not lead to a \mathcal{T} -symmetric physical wavefunction due to these swap gates. In this appendix, we will show that local \mathcal{T} constraint gives a symmetric physical wavefunction if and only if a hidden Kasteleyn orientation can be extracted from such local constraint.

Let us first introduce Kasteleyn orientation. For a given oriented graph, Kasteleyn orientation means that for any face in such graph, the number of clockwise-oriented edges bounding it must be odd. It has been proven that Kasteleyn

orientation exists for any planar graph with an even number of vertices⁴³. The choice of Kasteleyn orientation is far from unique: given an Kasteleyn orientation, one can obtain another one by flipping arrows on all edges connecting a given vertex v . For each vertex, one can choose to flip or not to flip arrows on edges connecting this vertex, and it exhausts all possible choices of Kasteleyn orientation. Thus, there are total 2^{N_v} choices, where N_v is the total number of vertices.

We now turn to the honeycomb example in the main text. Let us explain rules to extract orientation from action of $W(\mathcal{T})$'s on local tensors. We first expand all sites of the honeycomb lattice to triangles as



Vertices in the new lattice live on internal legs of the honeycomb fPEPS, and thus can be labeled as $(s\alpha)$. Arrows on blue triangles in Eq. (S17) are extracted from \mathcal{T} -action on site tensors, while arrows on magenta lines in Eq. (S17) of the original hexagons from \mathcal{T} -action on bond tensors. More specifically, from \mathcal{T} -symmetric condition in the main text, for \mathcal{T} -action on tensor at site s

$$U_s(\mathcal{T}) \cdot \hat{T}_s^* = [W_{(s\alpha)}(\mathcal{T}) \otimes_f W_{(s\beta)}(\mathcal{T}) \otimes_f W_{(s\gamma)}(\mathcal{T})]^{-1} \cdot \hat{T}_s, \quad (\text{S18})$$

the arrows on the corresponding blue triangle is $(s\alpha) \rightarrow (s\beta)$, $(s\beta) \rightarrow (s\gamma)$, and $(s\alpha) \rightarrow (s\gamma)$. For example,

$$U_s(\mathcal{T}) \cdot \hat{T}_s^* = [W_{(sx)}(\mathcal{T}) \otimes_f W_{(sy)}(\mathcal{T}) \otimes_f W_{(sz)}(\mathcal{T})]^{-1} \cdot \hat{T}_s \Rightarrow \begin{array}{c} z \\ \nearrow \quad \searrow \\ x \quad \quad y \end{array}. \quad (\text{S19})$$

If \mathcal{T} -action on bond tensor $\hat{B}_{ss'}$ reads

$$V_{(\alpha 0)}(\mathcal{T}) \otimes_f V_{(\alpha 1)}(\mathcal{T}) \cdot (\hat{B}_{ss'})^* = \hat{B}_{ss'} \cdot W_{(s\alpha)}(\mathcal{T}) \otimes_f W_{(s'\alpha)}(\mathcal{T}), \quad (\text{S20})$$

the arrow is drawn from $(s\alpha)$ to $(s'\alpha)$. Following this rule, \mathcal{T} -symmetry constraint in the main text leads to the oriented graph in Eq. (S17), and one can check that it indeed gives one Kasteleyn orientation.

In the following, let us prove that the physical wavefunction is \mathcal{T} -symmetric only when the right hand side of Eq. (S17) is a Kasteleyn orientation. According to Eq. (16), the commutator between $W(\mathcal{T})$ and parity F reads

$$W^*(\mathcal{T}) \cdot F \cdot [W^{-1}(\mathcal{T})]^* = D \cdot F, \quad \text{where } D = \exp[i\pi n_D^*] \quad (\text{S21})$$

Here, D can be expressed as $P_e - P_o$, where $P_{e/o}$ are projectors to internal states without/with Ising domain wall. Using these projectors, we can decompose site and bond tensors to orthogonal sectors, e.g. $P_{e,x} \otimes_f P_{o,y} \otimes_f P_{o,z} \cdot \hat{T}$. By inserting $P_e + P_o$ on all internal legs of the tensor network wavefunction, the wavefunction equals summation of tensor contractions for different sectors. However, as D is an IGG element of the tensor network, local tensors vanish if acted by odd number of P_o 's. So, for the whole tensor network, action of P_o must form loops, which gives domain wall loops on physical legs after contraction. For any loops configuration d , we act P_o 's on internal legs along loops and P_e 's on internal legs within domains, and then obtain site tensors $\hat{T}^{d'}$'s and bond tensors $\hat{B}^{d'}$'s. By contracting internal legs of $\hat{T}^{d'}$'s and $\hat{B}^{d'}$'s, we get physical state $|\psi_d\rangle$, and physical wavefunction can be expressed as $|\Psi\rangle = \sum_d |\psi_d\rangle$.

In the following, we will prove that $\forall d, \mathcal{T}|\psi_d\rangle = |\psi_d\rangle$ if there is hidden Kasteleyn orientation, and thus $|\Psi\rangle$ is invariant under \mathcal{T} .

Let us start from configuration d without any loop. In this case, we only get $W_e(\mathcal{T})$'s when acting \mathcal{T} , which are parity even and free to permute. $|\psi_d\rangle$ is apparently invariant under \mathcal{T} : $\mathcal{T}|\psi_d\rangle = |\psi_d\rangle$.

For configuration d with a single loop, let the number of internal ket legs to be $2L$. We label internal legs along this loop counter-clockwise by l , and assume site tensors sitting between $l = 2k - 1$ and $l = 2k$. Site tensors along this loop for $|\psi_d\rangle$ can then be named as $\hat{T}_{2k-1,2k}^d$, while bond tensors as $\hat{B}_{2k,2k+1}^d$. As all tensors are parity even, we rearrange tensors along the loop together in the following way:

$$|\psi_d\rangle = \text{fTr}[\cdots \otimes_f \hat{B}_{2,3}^d \otimes_f \hat{B}_{3,4}^d \otimes_f \cdots \otimes_f \hat{B}_{2L,1}^d \otimes_f \hat{T}_{2L-1,2L}^d \otimes_f \hat{T}_{2L-3,2L-2}^d \otimes_f \cdots \otimes_f \hat{T}_{1,2}^d \otimes_f \cdots] \quad (\text{S22})$$

We now acting \mathcal{T} on $|\psi_d\rangle$, and according to Eq. (S18) and Eq. (S20), it equals action of $W(\mathcal{T})$'s on internal legs of \hat{T}^d 's and \hat{B}^d 's. We define $W_{e/o}(\mathcal{T}) \equiv P_{e/o} \cdot W(\mathcal{T})$, which is parity even/odd sector of $W(\mathcal{T})$. From definition of $|\psi_d\rangle$, $W(\mathcal{T})$'s act as $W_o(\mathcal{T})$'s on internal legs along the loop, while acting as $W_e(\mathcal{T})$'s on internal legs away from the loop. Fermion signs come from permuting $W_o(\mathcal{T})$'s and $[W_o(\mathcal{T})]^{-1}$'s, and thus we focus on contraction of $W(\mathcal{T})$'s along the loop. We arrange the order of $W_o(\mathcal{T})$'s contraction according to Eq. (S22) as

$$\begin{aligned} & \text{fTr} \left\{ \left((-1)^{s_{2,3}} \cdot W_{o,2}(\mathcal{T}) \otimes_f W_{o,3}(\mathcal{T}) \right) \otimes_f \cdots \otimes_f \left((-1)^{s_{2L,1}} \cdot W_{o,2L}(\mathcal{T}) \otimes_f W_{o,1}(\mathcal{T}) \right) \bigotimes_f \right. \\ & \quad \left. \left[\left((-1)^{s_{1,2}} \cdot W_{o,1}(\mathcal{T}) \otimes_f W_{o,2}(\mathcal{T}) \right) \otimes_f \cdots \otimes_f \left((-1)^{s_{2L-1,2L}} \cdot W_{o,2L-1}(\mathcal{T}) \otimes_f W_{o,2L}(\mathcal{T}) \right) \right]^{-1} \right\} \\ & = (-1)^{1+\sum_l s_{l,l+1}} = 1 \end{aligned} \quad (\text{S23})$$

where $s_{l,l+1} = 0/1$ if the arrow at $(l, l+1)$ is along/against the direction of the loop (counter-clockwise/clockwise direction). The last equation is from the definition of Kasteleyn orientation: there are always odd number of arrows against direction of the loop. So, for configuration d with a single loop, $W(\mathcal{T})$'s and $[W(\mathcal{T})]^{-1}$'s cancels, and $|\psi_d\rangle$ is \mathcal{T} -symmetric. In contrast, if the orientation is not Kasteleyn, one can always find a loop configuration d , such that the last line of Eq. (S23) gives -1 . So, $|\Psi\rangle$ breaks \mathcal{T} symmetry if there is no Kasteleyn orientation.

For configuration d with more than one loops, we can arrange all tensors belonging to one loop together, and repeat the above calculation for every loop. Thus, such $|\psi_d\rangle$ is also \mathcal{T} -symmetric. In conclusion, $|\Psi\rangle$ is \mathcal{T} -symmetric if and only if the orientation extracted from $W(\mathcal{T})$'s is a Kasteleyn orientation.

As we mentioned in the beginning of this part, by flipping arrows on all edges connecting to certain vertices, one gets another Kasteleyn orientation. In the tensor language, flipping arrows for edges connecting to vertex $(s\alpha)$ corresponds to modifying $W_{(s\alpha)}(\mathcal{T})$ to $D_{(s\alpha)} \cdot W_{(s\alpha)}(\mathcal{T})$. To see this, we consider the following \mathcal{T} -action on site tensors:

$$[D_{(sx)} \cdot W_{(sx)}(\mathcal{T}) \otimes_f W_{(sy)}(\mathcal{T}) \otimes_f W_{(sz)}(\mathcal{T})]^{-1} \cdot \hat{T}_s = [W_{(sy)}(\mathcal{T}) \otimes_f W_{(sz)}(\mathcal{T}) \otimes_f W_{(sx)}(\mathcal{T})]^{-1} \cdot \hat{T}_s \Rightarrow \begin{array}{c} z \\ \swarrow \quad \searrow \\ x \quad y \end{array}$$

Similar logic works for bond tensors. Following these rules for arrows, there is one-to-one correspondence between gauge transformation $W(\mathcal{T})$ and Kasteleyn orientation.

We focus on trivalent lattice in the above argument, where each vertex connects three bonds, and there is at most one domain wall travelling through a vertex. We now generalize the above argument to generic lattices, where more than one domain walls may meet at sites.

Let us present rules for extract orientations in such generic lattices. Similar as Eq. (S17), we first construct a new planar graph, where a site connecting n -bonds in the original lattice splits to n vertices in the new graph, and each vertex is labeled by the internal leg index. Each pair of these n vertices are connected by new edges. Given \mathcal{T} -action on internal legs, arrows on edges of the new planar graph follows similar rules presented in Eq. (S19) and Eq. (S20). For example, consider site tensor s with four internal legs, the above rule reads

$$U(\mathcal{T}) \cdot \hat{T}_s^* = [W_{(sa)}(\mathcal{T}) \otimes_f W_{(sb)}(\mathcal{T}) \otimes_f W_{(sc)}(\mathcal{T}) \otimes_f W_{(sd)}(\mathcal{T})]^{-1} \cdot \hat{T}_s \Rightarrow \begin{array}{c} b \\ \swarrow \quad \searrow \\ a \quad c \\ \nwarrow \quad \nearrow \\ d \end{array}$$

To proceed, let us focus on a particular choice of Kasteleyn orientation. We number the n vertices from 1 to n clockwise, and let the arrow pointing from i to j if $i < j$. It is easy to verify that any loop within these n vertices matches the condition for Kasteleyn orientation. Arrows on bond tensors are chosen to satisfy conditions for Kasteleyn orientation with larger loops.

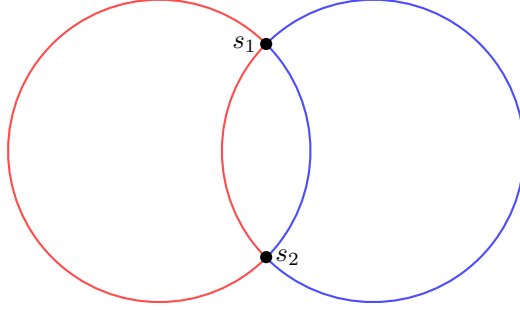


FIG. 4. Two domain wall loops (red and blue) intersect at site s_1 and s_2 . Here, $s_{1,2}$ are not “true crossing points” of these two loops: they are separate at these two points.

For loops configurations without loop crossing, using similar argument presented in the honeycomb lattice case, we conclude that $W(\mathcal{T})$'s cancels without additional sign.

As shown in Fig. 4, we consider configuration d where two loops (colored blue and red) intersect at site s_1 and s_2 . Loops are chosen such that internal legs belonging to one loop are neighbour of each other. Thus, there are no “true crossing points” between these two loops.

By inserting P_o 's on internal legs at these two loops, and P_e 's on other internal legs, we obtain tensors \hat{T}^{d_i} 's and \hat{B}^{d_i} 's, and wavefunction $|\psi_d\rangle$ from contracting \hat{T}^{d_i} 's and \hat{B}^{d_i} 's. Let the number of internal ket legs of the red/blue loop to be $2L_1/2L_2$. We label internal legs along these two loops by index l , where $1 \leq l \leq 2L_1$ labels internal legs along the red loop and $2L_1 + 1 \leq l \leq 2L_1 + 2L_2$ for the blue loop. Due to the intersecting sites $s_{1/2}$, Eq. (S22) do not directly apply to the case here. However, at any intersection point, two W_o^{-1} 's belonging to one loop always come together (or can be moved together without sign). Thus, we can always move all W_o^{-1} 's belonging to one loop together without extra sign, and Eq. (S23) still applies for every single loop. The above argument can be easily generalized to any loop configurations. We then conclude that for a \mathcal{T} symmetric fPEPS of the QSH phase in any lattice, the planar graph extracted from $W(\mathcal{T})$'s satisfies Kasteleyn orientation.

IV. $\mathcal{T}^2 = F$ ON INTERNAL LEGS

In this part, we show that Eq. (18) is consistent with $\mathcal{T}^2 = F$ when acting on tensors. We consider a tensor \hat{T}_A with L internal bra legs and physical Hilbert space \mathbb{H}_A . According to the main text, the \mathcal{T} -symmetric condition for \hat{T}_A reads

$$U_A(\mathcal{T}) \cdot \hat{T}_A^* = \hat{T}_A \cdot \bigotimes_{j=1}^L W_j(\mathcal{T}) \quad (\text{S24})$$

By acting \mathcal{T} twice, we obtain

$$F_A \cdot \hat{T}_A = U_A(\mathcal{T}) \cdot U_A^*(\mathcal{T}) \cdot \hat{T}_A = \hat{T}_A \cdot \left(\bigotimes_{j=1}^L W_j(\mathcal{T}) \right) \cdot \left(\bigotimes_{j=1}^L W_j^*(\mathcal{T}) \right) \quad (\text{S25})$$

Due to the unfixed parity of $W(\mathcal{T})$'s, one cannot permute $W(\mathcal{T})$'s directly. Instead, from Eq. (S21), we have

$$\begin{aligned} F_A \cdot \hat{T}_A &= \hat{T}_A \cdot \left(\bigotimes_{j=1}^L W_j(\mathcal{T}) \right) \cdot \left(\bigotimes_{j=1}^L W_j^*(\mathcal{T}) \right) \\ &= \hat{T}_A \cdot \bigotimes_{j=1}^L (-)^{n_{D,j}} \sum_{k < j} n_{D,k} W_j(\mathcal{T}) \cdot W_j^*(\mathcal{T}) = \hat{T}_A \cdot (-)^{\sum_{k < j} n_{D,k} n_{D,j}} \bigotimes_{j=1}^L W_j(\mathcal{T}) \cdot W_j^*(\mathcal{T}) \\ &= \hat{T}_A \cdot e^{-i \frac{\pi}{2} \sum_{j \neq k} n_{D,k} n_{D,j}} \bigotimes_{j=1}^L W_j(\mathcal{T}) \cdot W_j^*(\mathcal{T}) = \hat{T}_A \cdot \bigotimes_{j=1}^L e^{i \frac{\pi}{2} n_{D,j}^2} W_j(\mathcal{T}) \cdot W_j^*(\mathcal{T}), \end{aligned} \quad (\text{S26})$$

where the last line comes from the condition that $\sum_j n_{D,j} = 0$. Then on each internal leg we have

$$\exp\left[i\frac{\pi}{2}n_D^2\right] \cdot W(\mathcal{T}) \cdot W^*(\mathcal{T}) = F \quad (\text{S27})$$

or at most differ from F up to an IGG element. So, by acting $\mathcal{T}^2 = F$ on internal legs of tensors, we get consistent result as Eq. (18).

V. EDGE THEORIES FROM INFINITE PEPS

In this appendix, we will identify Hilbert space and symmetry action of the edge theory from infinite PEPS.

We cut a finite region A from an infinite PEPS. By contracting all internal legs within A , we obtain a linear map \hat{T}_A from virtual legs at boundary of A – labeled as $\mathbb{H}_{\partial A}$ – to physical legs in the bulk of A – labeled as \mathbb{H}_A :

$$\hat{T}_A = \sum \langle T_A \rangle_{i_b i_e} |i_b\rangle \langle i_e|, \quad |i_b\rangle \in \mathbb{H}_A, \quad \langle i_e| \in \mathbb{H}_{\partial A} \quad (\text{S28})$$

Here, without loss of generality, we choose all boundary legs to be bra spaces. For large enough region A , $\dim \mathbb{H}_A \gg \dim \mathbb{H}_{\partial A}$, so the map can never be surjective.

We can write down a symmetric Hamiltonian for a system on A , whose low-energy space is image of \hat{T}_A , which is isomorphic to $\mathbb{H}_{\partial A} / \ker \hat{T}_A$. As bulk excitations are gapped, low energy states are identified as edge modes, and thus $\mathbb{H}_{edge} \cong \mathbb{H}_{\partial A} / \ker \hat{T}_A$.

If \hat{T}_A is injective, $\mathbb{H}_{edge} = \mathbb{H}_{\partial A}$, and it naturally leads to a tensor product structure of the edge Hilbert space. If IGG is nontrivial, \hat{T}_A will no longer be injective. Given an IGG element whose action on ∂A is $J_{\partial A}$, according to the definition of IGG, $T_A \cdot (\hat{1}_{\partial A} - J_{\partial A}) = 0$, and we have $\ker \hat{T}_A \supset \text{imag}(\hat{1}_{\partial A} - J_{\partial A}) \neq 0$.

In this work, we further assume that $\ker \hat{T}_A = \{\text{imag}(\hat{1}_{\partial A} - J_{\partial A}) | \forall J \in \text{IGG}\}$. In other words, *IGG determines the edge Hilbert space*:

$$\mathbb{H}_{edge} = \{|\psi_{\partial A}\rangle \mid J_{\partial A}|\psi_{\partial A}\rangle = |\psi_{\partial A}\rangle, \forall J \in \text{IGG}\} \quad (\text{S29})$$

We define $\hat{T}_A^{-1} : \mathbb{H}_A \rightarrow \mathbb{H}_{\partial A}$ as pseudo-inverse of \hat{T}_A , which satisfies

$$\hat{T}_A \cdot \hat{T}_A^{-1} = P_l, \quad \hat{T}_A^{-1} \cdot \hat{T}_A = P_{edge}, \quad (\text{S30})$$

where P_l is the projector from \mathbb{H}_A to $\text{imag} \hat{T}_A$, while P_{edge} is the projector from $\mathbb{H}_{\partial A}$ to \mathbb{H}_{edge} .

In the following, let us work out how symmetries act on edge. Here, we focus on onsite symmetry group G . For $g \in G$, we have

$$U_A(g) \mathcal{K}^{s(g)} \cdot T_A = T_A \cdot W_{\partial A}(g) \mathcal{K}^{s(g)} \quad (\text{S31})$$

So, it is natural to identify $U_{edge}(g) \mathcal{K}^{s(g)} \equiv P_{edge} \cdot W_{\partial A}(g) \mathcal{K}^{s(g)} \cdot P_{edge}$ as symmetry action on \mathbb{H}_{edge} .

Note that $\forall J \in \text{IGG}$, we have

$$U_A(g) \mathcal{K}^{s(g)} \cdot \hat{T}_A = \hat{T}_A \cdot W_{\partial A} \mathcal{K}^{s(g)} = U_A(g) \mathcal{K}^{s(g)} \cdot \hat{T}_A \cdot J_{\partial A} = \hat{T}_A \cdot W_{\partial A} \mathcal{K}^{s(g)} \cdot J_{\partial A} \quad (\text{S32})$$

Together with Eq. (S29), we conclude

$$U_{edge}(g) \mathcal{K}^{s(g)} = P_{edge} \cdot W_{\partial A}(g) \mathcal{K}^{s(g)} = W_{\partial A}(g) \mathcal{K}^{s(g)} \cdot P_{edge} \quad (\text{S33})$$

VI. FUSION OF \mathcal{T} -FLUX

As in Appendix V, let us consider a region A described by a large tensor \hat{T}_A with physical Hilbert space \mathbb{H}_A and boundary legs $\mathbb{H}_{\partial A}$, where legs at ∂A are labeled by $j = \{1, 2, \dots, L\}$.

We create \mathcal{T} -flux at $j = 1$ and $l+1$ by inserting a charge-neutral operator $U_M(\mathcal{T}) \mathcal{K} \equiv P_{edge} \cdot w_{l+1} \cdot w_1 \cdot W_M(\mathcal{T}) \mathcal{K} \cdot P_{edge}$, where $M = \{2, 3, \dots, l\} \in \partial A$. Here, $w_{1/(l+1)}$ are local operators at the ends and

$$W_M(\mathcal{T}) = \bigotimes_{j=2}^l W_j(\mathcal{T})$$

We choose $w_{1/(l+1)}$ such that $w_{l+1} \cdot w_1 \cdot W_M(\mathcal{T})\mathcal{K}$ commute with P_{edge} .

To make $U_M(\mathcal{T})\mathcal{K}$ charge neutral, we require commutator between $w_{1/(l+1)}$ and n_f to be

$$[w_1, n_{f;1}] = n_{\lambda; \frac{3}{2}}^{(0)} \cdot w_1 ; \quad [w_{l+1}, n_{f;l+1}] = n_{\lambda; l+\frac{1}{2}}^{(1)} \cdot w_{l+1} \quad (\text{S34})$$

The charge neutral condition is satisfied as $[W_j(\mathcal{T}), n_{f;j}] = n_{D;j} \cdot W_j(\mathcal{T})$ and $\left(n_{\lambda; \frac{3}{2}}^{(0)} + n_{\lambda; l+\frac{1}{2}}^{(1)} + \sum_{j=2}^l n_{D;j}\right) \cdot P_{edge} = 0$.

We now calculate fusion of two \mathcal{T} -flux. Without loss of generality, we assume that $j=1$ and $j=l+1$ legs belong to v -sublattice. By performing similar derivation presented in Eq. (S26), we have

$$U_M(\mathcal{T}) \cdot U_M^*(\mathcal{T}) = P_{edge} \cdot e^{i \frac{\pi}{2} \left(n_{\lambda; l+\frac{1}{2}}^{(1)}\right)^2} w_{l+1} \cdot w_{l+1}^* \otimes_f e^{i \frac{\pi}{2} \left(n_{\lambda; \frac{3}{2}}^{(0)}\right)^2} w_1 \cdot w_1^* \bigotimes_{f, j=2}^l e^{i \frac{\pi}{2} n_{D;j}^2} W_j(\mathcal{T}) \cdot W_j^*(\mathcal{T}) \cdot P_{edge} . \quad (\text{S35})$$

As $\left(n_{\lambda; l+\frac{1}{2}}^{(1)}\right)^2 = -n_{\lambda; l+\frac{1}{2}}^{(1)}$ and $\left(n_{\lambda; \frac{3}{2}}^{(0)}\right)^2 = n_{\lambda; \frac{3}{2}}^{(0)}$, we obtain

$$(U_M(\mathcal{T})\mathcal{K})^2 = P_{edge} \cdot \Omega_{l+1} \Omega_1 \cdot \prod_{j=2}^l F_j \cdot P_{edge} , \quad (\text{S36})$$

Here,

$$\Omega_{l+1} = P_{edge} \cdot e^{-i \frac{\pi}{2} n_{\lambda; l+\frac{1}{2}}^{(1)}} w_{l+1} \cdot w_{l+1}^* \cdot P_{edge} = e^{-i \frac{\pi}{2} n_{\lambda; l+\frac{1}{2}}^{(1)}} c_{l+1}^\dagger , \quad (\text{S37})$$

$$\Omega_1 = P_{edge} \cdot e^{i \frac{\pi}{2} n_{\lambda; \frac{3}{2}}^{(0)}} w_1 \cdot w_1^* \cdot P_{edge} = e^{i \frac{\pi}{2} n_{\lambda; \frac{3}{2}}^{(0)}} c_1 . \quad (\text{S38})$$

where we use Eq. (24) to fix the final form of $\Omega_{1/(l+1)}$.

VII. VARIATIONAL ANSATZ FOR THE QSH PHASE ON SQUARE LATTICE SPIN-1/2 ELECTRONIC SYSTEM

In this section, we present detailed derivation for solving tensor equations on a spin- $\frac{1}{2}$ fermionic system on the bipartite square lattice. Each site tensor has four internal legs and one physical spin- $\frac{1}{2}$ fermion, which is represented as

$$|i\rangle_1 \downarrow, |k\rangle_3 \uparrow, |l\rangle_4 \rightarrow, |p\rangle_2 \leftarrow \quad \text{Tensor} \quad = T_{ijkl,p} |i\rangle_1 |j\rangle_2 |k\rangle_3 |l\rangle_4 |p\rangle .$$

Sites on the bipartite square lattice can be grouped to two types, where we use $\hat{T}_{u/v}$ to label site tensors on different sublattices. Physical legs are spin-1/2 fermions f_σ , and charges carried by f_σ 's are opposite in u - and v -site. As in the honeycomb example, an internal leg ($s\alpha$) can also be represented by a triple-line, where the middle line is a spinless fermion mode $c_{(s\alpha)}$, and two side lines are Ising spins $|\tau\rangle_{(s\alpha)}$, where $s = u/v$, $\alpha \in \{1, 2, 3, 4\}$ and $a = 0/1$. Orders of a is counter-clockwise/clockwise for site u/v . For simplicity, we focus on four of eight basis states: $\{|\uparrow\uparrow\rangle_{(s\alpha)}, c_{(s\alpha)}^\dagger |\uparrow\downarrow\rangle_{(s\alpha)}, |\downarrow\uparrow\rangle_{(s\alpha)}, |\downarrow\downarrow\rangle_{(s\alpha)}\}$.

Symmetry constraints on site tensor \hat{T}_s are

$$\bigotimes_{\alpha=1}^4 W_{(s\alpha)}(\mathcal{T}) \otimes_f U_s(\mathcal{T}) \cdot \hat{T}_s^* = \hat{T}_s$$

$$\left[\sum_{\alpha=1}^4 n_{f;(s\alpha)} + n_{f;s} \right] \cdot \hat{T}_s = 0 \quad (\text{S39})$$

where $W(\mathcal{T})$, n_f , and n_λ take the same form as those in the honeycomb example. To take care of sign factors when acting $W(\mathcal{T})$'s on site tensor \hat{T}_s , a Jordan-Wigner string $J = \exp\{i\pi n_f\}$ is introduced. Then, the “bosonized” $W(\mathcal{T})$ is

$$W_{(sj)}^b(\mathcal{T}) = P_e \cdot W_{(sj)}(\mathcal{T}) + \bigotimes_{k=1}^{j-1} J_k \otimes P_o \cdot W_{(sj)}(\mathcal{T}), \quad (\text{S40})$$

\mathcal{T} symmetry constraint on a site tensor gives

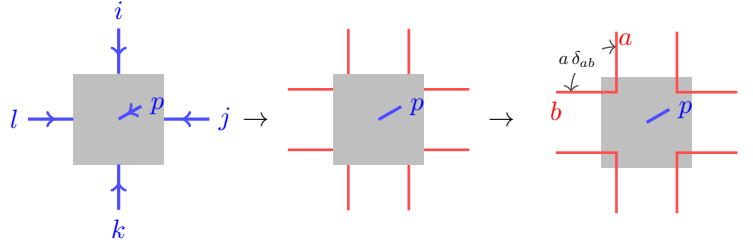
$$\prod_{\alpha=1}^4 W_{(s\alpha)}^b(\mathcal{T}) \cdot U(\mathcal{T}) \cdot T_s^* = T_s \quad (\text{S41})$$

Here T_s without hat is a “bosonic tensor” with entries $(T_s)_{\alpha\beta\gamma\delta,p}$.

Site tensor \hat{T} should also satisfy the plaquette IGG condition:

$$\left(n_{\lambda;(s\alpha 0)} + n_{\lambda;(s\tilde{\alpha} 1)}\right) \cdot \hat{T}_s = 0, \quad \forall \alpha. \quad (\text{S42})$$

where $\tilde{\alpha} = \alpha + (-1)^s$. This equation identifies internal states within a plaquette:



The dimension of the tensor T_s is 1024, and after solving the tensor equations in Eq. (S39) and (S42) there are only 14 linearly independent solutions. And the solution for \hat{T}_v reads

$$\hat{T}_v = \sum_l^{14} c_l \hat{t}_l, \quad (\text{S43})$$

where c_l 's are real numbers, and \hat{t}_l can be represented graphically as

$$\begin{aligned} t_1 &= \begin{array}{c} \downarrow \downarrow \downarrow \\ \rightarrow 0 \leftarrow \\ \uparrow \uparrow \uparrow \end{array} + \begin{array}{c} \downarrow \downarrow \downarrow \\ \rightarrow 0 \leftarrow \\ \uparrow \uparrow \uparrow \end{array}; \quad t_2 = \begin{array}{c} \downarrow \downarrow \downarrow \\ \rightarrow \uparrow \leftarrow \\ \uparrow \uparrow \uparrow \end{array} + \begin{array}{c} \downarrow \downarrow \downarrow \\ \rightarrow \uparrow \leftarrow \\ \uparrow \uparrow \uparrow \end{array}; \quad t_3 = \begin{array}{c} \downarrow \downarrow \downarrow \\ \rightarrow \uparrow \leftarrow \\ \uparrow \uparrow \uparrow \end{array} + \begin{array}{c} \downarrow \downarrow \downarrow \\ \rightarrow \uparrow \leftarrow \\ \uparrow \uparrow \uparrow \end{array}; \quad t_4 = \begin{array}{c} \downarrow \downarrow \downarrow \\ \rightarrow \uparrow \leftarrow \\ \uparrow \uparrow \uparrow \end{array} - \begin{array}{c} \downarrow \downarrow \downarrow \\ \rightarrow \uparrow \leftarrow \\ \uparrow \uparrow \uparrow \end{array}; \\ t_5 &= \begin{array}{c} \uparrow \uparrow \uparrow \\ \rightarrow \downarrow \leftarrow \\ \downarrow \downarrow \downarrow \end{array} + \begin{array}{c} \uparrow \uparrow \uparrow \\ \rightarrow \downarrow \leftarrow \\ \downarrow \downarrow \downarrow \end{array}; \quad t_6 = \begin{array}{c} \uparrow \uparrow \uparrow \\ \rightarrow \downarrow \leftarrow \\ \downarrow \downarrow \downarrow \end{array} - \begin{array}{c} \uparrow \uparrow \uparrow \\ \rightarrow \downarrow \leftarrow \\ \downarrow \downarrow \downarrow \end{array}; \quad t_7 = \begin{array}{c} \uparrow \uparrow \uparrow \\ \rightarrow \downarrow \leftarrow \\ \downarrow \downarrow \downarrow \end{array} + \begin{array}{c} \uparrow \uparrow \uparrow \\ \rightarrow \downarrow \leftarrow \\ \downarrow \downarrow \downarrow \end{array}; \quad t_8 = \begin{array}{c} \uparrow \uparrow \uparrow \\ \rightarrow \downarrow \leftarrow \\ \downarrow \downarrow \downarrow \end{array} - \begin{array}{c} \uparrow \uparrow \uparrow \\ \rightarrow \downarrow \leftarrow \\ \downarrow \downarrow \downarrow \end{array}; \\ t_9 &= \begin{array}{c} \downarrow \downarrow \downarrow \\ \rightarrow \uparrow \leftarrow \\ \uparrow \uparrow \uparrow \end{array} - \begin{array}{c} \downarrow \downarrow \downarrow \\ \rightarrow \uparrow \leftarrow \\ \uparrow \uparrow \uparrow \end{array}; \quad t_{10} = \begin{array}{c} \downarrow \downarrow \downarrow \\ \rightarrow \uparrow \leftarrow \\ \uparrow \uparrow \uparrow \end{array} + \begin{array}{c} \downarrow \downarrow \downarrow \\ \rightarrow \uparrow \leftarrow \\ \uparrow \uparrow \uparrow \end{array}; \quad t_{11} = \begin{array}{c} \downarrow \downarrow \downarrow \\ \rightarrow \uparrow \leftarrow \\ \uparrow \uparrow \uparrow \end{array} - \begin{array}{c} \downarrow \downarrow \downarrow \\ \rightarrow \uparrow \leftarrow \\ \uparrow \uparrow \uparrow \end{array}; \quad t_{12} = \begin{array}{c} \downarrow \downarrow \downarrow \\ \rightarrow \uparrow \leftarrow \\ \uparrow \uparrow \uparrow \end{array} + \begin{array}{c} \downarrow \downarrow \downarrow \\ \rightarrow \uparrow \leftarrow \\ \uparrow \uparrow \uparrow \end{array}; \\ t_{13} &= \begin{array}{c} \uparrow \uparrow \uparrow \\ \rightarrow \downarrow \leftarrow \\ \downarrow \downarrow \downarrow \end{array} - \begin{array}{c} \uparrow \uparrow \uparrow \\ \rightarrow \downarrow \leftarrow \\ \downarrow \downarrow \downarrow \end{array}; \quad t_{14} = \begin{array}{c} \uparrow \uparrow \uparrow \\ \rightarrow \downarrow \leftarrow \\ \downarrow \downarrow \downarrow \end{array} + \begin{array}{c} \uparrow \uparrow \uparrow \\ \rightarrow \downarrow \leftarrow \\ \downarrow \downarrow \downarrow \end{array}. \end{aligned}$$

Magenta arrow indicates a fermion on the internal leg. \hat{T}_u 's solution is given by flipping all plaquette Ising spins of \hat{T}_v .

Now, let us discuss the bond tensors. As shown in Appendix III, to make the tensor network \mathcal{T} symmetric, \mathcal{T} action on bonds should be chosen to satisfy Kasteleyn orientation:

$$\hat{B}_\alpha \cdot W_{(u\alpha)}(\mathcal{T}) \otimes_f W_{(v\beta)}(\mathcal{T}) = \hat{B}_\alpha^* \quad (\text{S44})$$

Here, we impose rotational symmetry, and thus all four types of bond tensors share the same form:

$$\begin{array}{c} (\beta|_v \\ \uparrow \\ \boxed{B} \\ \downarrow \\ (\alpha|_u \end{array} = \begin{array}{c} (\alpha|_u \leftarrow \boxed{B} \rightarrow (\beta|_v \end{array} = \begin{array}{c} (\alpha|_u \\ \uparrow \\ \boxed{B} \\ \downarrow \\ (\beta|_v \end{array} = \begin{array}{c} (\beta|_v \rightarrow \boxed{B} \leftarrow (\alpha|_u \end{array} = B_{\alpha\beta} (\alpha| (\beta| \quad (\text{S45})$$

Bond tensors should also be invariant under plaquette IGG:

$$\left(n_{\lambda;(u\alpha a)} + n_{\lambda;(v\alpha a)} \right) \cdot \hat{B}_\alpha = 0, \quad \forall \alpha \text{ \& } a, \quad (\text{S46})$$

which identifies the internal states within a plaquette:

$$\begin{array}{c} \text{---} \end{array} \boxed{B} \begin{array}{c} \text{---} \end{array} \rightarrow \begin{array}{c} \text{---} \\ \boxed{B} \\ \text{---} \end{array} \rightarrow \begin{array}{c} \text{---} \\ \boxed{B} \\ \text{---} \end{array}. \quad (\text{S47})$$

By further imposing charge neutral condition, we get solution for \hat{B}_α as

$$\hat{B}_\alpha = d_e \hat{b}_e + d_o \hat{b}_o, \quad (\text{S48})$$

where $\hat{b}_e = (\uparrow\uparrow|_u (\uparrow\uparrow|_v + (\downarrow\downarrow|_u (\downarrow\downarrow|_v$, and $\hat{b}_o = (\uparrow\downarrow|_u (\uparrow\downarrow|_v c_u c_v - (\downarrow\uparrow|_u (\downarrow\uparrow|_v$. Here, $d_{e/o}$ are real parameters. By performing gauge transformation, we can always absorb d 's to site tensors and simply set $d_e = d_o = 1$. Namely, bond tensors are maximal entangled states, which share the same form as Eq. (12).